ACS APPLIED MATERIALS & INTERFACES

Research Article

Cite This: ACS Appl. Mater. Interfaces 2019, 11, 43351−43358

www.acsami.org

UV Rewritable Hybrid Graphene/Phosphor p−n Junction Photodiode

Hao Li,[†] Shubin Su,[†] Chenhui Liang,[†] Ting Zhang,[‡] Xuhong An,[§] Meizhen Huang,[†] Haihua Tao,*[,†] Xiang Ma,[‡] Zhenhua Ni,[§] He Tian,[‡] and Xianfeng Chen*[,†]

[†]State Key Laboratory of Advanced Optical Communication Systems and Networks, School of Physics and Astronomy, Shanghai Jiao Tong University, Shanghai 200240, China

[‡]Key Laboratory for Advanced Materials and Institute of Fine Chemicals, School of Chemistry and Molecular Engineering, East China University of Science & Technology, Shanghai 200237, China

[§]Department of Physics, Southeast University, Nanjing 211189, China

Supporting Information

ABSTRACT: Graphene-based p−n junction photodiodes have a potential application prospect in photodetection due to their broadband spectral response, large operating bandwidth, and mechanical flexibility. Here, we report an ultraviolet (UV) rewritable p−n junction photodiode in a configuration of graphene coated with an amorphous phosphor of 4-bromo-1,8-naphthalic anhydride derivative polymer (poly-BrNpA). Under moderate UV irradiation, occurrence of photoisomerization reaction in the poly-BrNpA film leads to its drastically modified optical characteristics and a concurrent n-type doping in the underneath graphene. Meanwhile, the poly-BrNpA film, highly sensitive to water molecules, has a capability of restoring graphene to its initial p-type doping status by means of water adsorption. Based on these findings, a lateral graphene/poly-BrNpA p−n junction photodiode, responsive to visible light at the junction interface, can be written by UV irradiation and then erased via water adsorption. The p−n junction photodiode is rewritable upon such repetitive loops showing repeatable optoelectronic properties. This study provides a new scheme and perspective of making graphene-based rewritable p−n junction photodiodes in a flexible and controllable way, and it may contribute to expanding new families of optoelectronic devices based on two-dimensional materials.

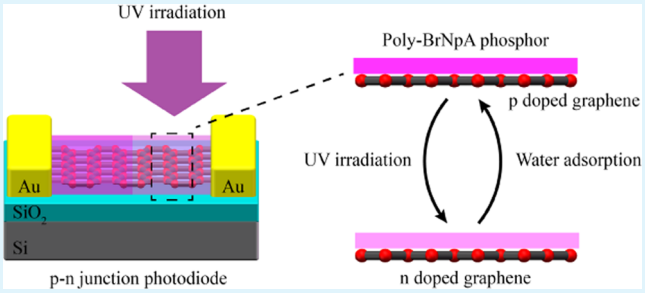

KEYWORDS: *graphene, photodiode, rewritable, phosphor, photoisomerization*

INTRODUCTION

Graphene-based lateral p−n junction photodiodes play a key role in the field of photodetection due to their inspiring features of broadband spectral response, large operating bandwidth, and mechanical flexibility.[1−10] In general, this type of p−n junctions are fabricated by two routes: one is to introduce heteroatoms through pretreating substrates or changing growth parameters in the chemical vapor deposition (CVD) process,[2,3] and the other is to introduce extra charge carriers in graphene via approaches like direct contact doping,[8] electrostatic gating,[4,11] and electron and light irradiations.[5−8,12−20] Among them, post-treatment of graphene under electron or light irradiation provides a feasible solution to realizing rewritable p−n junctions by virtue of reversible charge transfer, opening a door to a variety of graphene-based optoelectronic devices.[7,13−19]

Light irradiation has a capability of doping graphene in macro-/micro-/nanometer scale in a flexible and cost-effective way. On one hand, oxygen radicals photodissociated under vacuum ultraviolet (UV) irradiation, or high-energy-laser-induced heating at visible wavelengths, can cause photochemical oxidation and as a consequence induce irreversible charge doping in graphene.[5,6,8,20] On the other hand, under moderate UV or visible-light irradiations, photoexcited charges trapped at SiO_2 interface or defects situated inside hexagonal boron nitride (h-BN) can dope graphene via charge transfer in a reversible way.[15−19] This remarkable reversibility of charge carrier doping has the potential for making graphene-based rewritable photodetectors from the perspective of photons,[15−19] overcoming the limitation of nanomechanical fabrication by a scanning probe in complex-oxide materials.[21] As for graphene supported on SiO_2/Si substrates, however, its charge carrier restoration ensuing UV irradiation-induced doping appears too slow to be applied in the field of rewritable photodetectors.[15,18,19] Meanwhile, the gate-controllable photo-induced p−n junction in hybrid graphene/h-BN structure

Received: August 13, 2019
Accepted: October 28, 2019
Published: October 28, 2019

DOI: 10.1021/acsami.9b14461
ACS Appl. Mater. Interfaces 2019, 11, 43351−43358

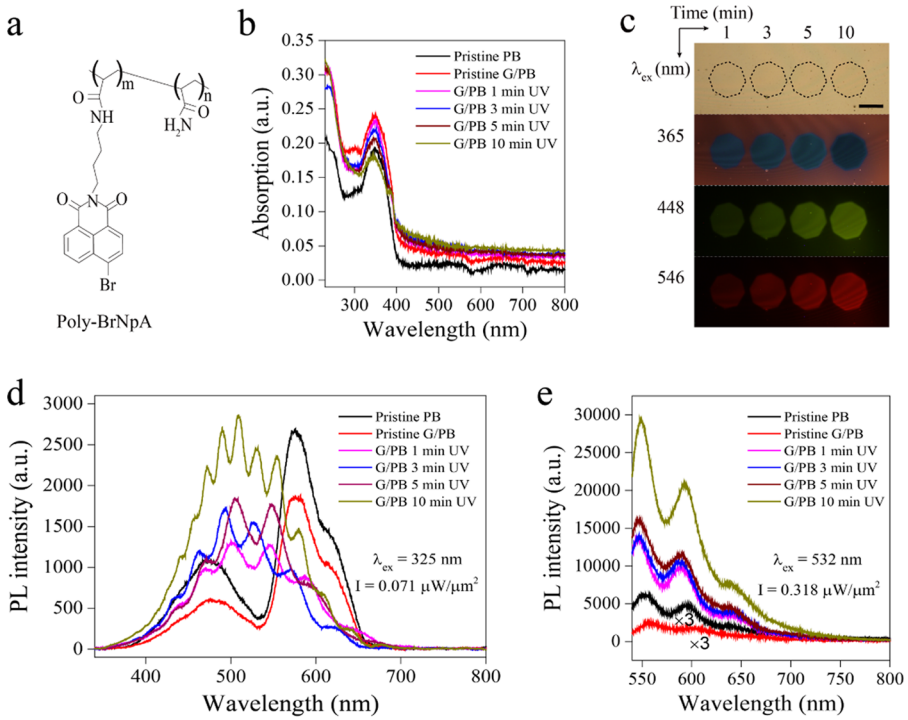

Figure 1. Characterization of the poly-BrNpA phosphor under UV irradiation. (a) Skeletal structural formula of the poly-BrNpA phosphor with the radio of m/n = 1:50. (b) UV−vis−NIR absorption spectral evolution for UV-irradiated poly-BrNpA film, (c) its PL images excited by UV−vis light (λ = 365, 448, and 546 nm), and its spectral evolution excited by lasers at (d) 325 nm and (e) 532 nm. The PL intensity of pristine PB and G/PB are multiplied by 3 for clarity. PB and G/PB in panels (b), (d), and (e) denote poly-BrNpA and graphene/poly-BrNpA, respectively. The scale bar in (c) is 100 μm.

appears challenging for photodetection due to its erasable character under daylight irradiation.[16,17]

Organic/inorganic photosensitive layer can improve the photoresponsivity of graphene-based hybrid photodetectors by functioning as a charge-transfer medium following its additional optical absorption.[6,9,10] Some kinds of organic fluorescent materials were recently demonstrated to possess fantastic optical features like photochromic behavior, paving the way for novel scientific studies and applications.[22−25] Metal-free room-temperature phosphor, a type of newly emerging organic luminescent material, has attracted more and more attention toward exploring new photoelectric devices in the last few years.[26−28] Compared with the popularly used fluorescent materials, it has much abundant electronic states and can emit an extra slow phosphorescence under optical excitation stemming from the triplet-to-singlet state electron transitions.[22−28] When combined with graphene, the peculiar electronic and optical traits of phosphor may provide a solution to realize graphene-based rewritable photodetectors.

In this work, we report a UV rewritable lateral p−n junction photodiode based on the hybrid graphene/4-bromo-1,8-naphthalic anhydride derivative polymer (poly-BrNpA) field-effect transistor (FET) structure.[28] Under moderate UV irradiation, the poly-BrNpA phosphor exhibits an interesting irreversible photoisomerization phenomenon with its optical absorption and photoluminescence (PL) properties drastically modified. As a result, it facilitates n-type doping conversion in the underneath graphene via interfacial electron transfer. A reverse charge doping is then realized by virtue of its high sensitivity to water molecules. In this process, a defect band is introduced in the band gap by water molecule adsorption, and it opens a channel for electrons reverting to the phosphor. By precisely tuning the UV spot size and its position irradiated on FET channels, we can make graphene/poly-BrNpA lateral p−n junction photodiodes. Such photodiodes can be erased by water molecule adsorption and exhibit rewritable and stable characteristics under the cyclic UV irradiations. This work opens the way to develop graphene-based rewritable photodiodes in a flexible way, and it may provide new perspectives to developing novel optoelectronics based on the flourishing two-dimensional materials.[29−33]

EXPERIMENTAL SECTION

Fabrication of the Hybrid Graphene/Poly-BrNpA FET Device. Large-area CVD-grown monolayer graphene was transferred from copper foil onto SiO_2 (300 nm)/Si (p^{++}, 0.001−0.004 Ω·cm) substrates taking a PMMA-mediated approach,[34−37] and then annealed in a flowing gas mixture (Ar/H_2 = 200:100 sccm) for 2 h at 290 °C. The hybrid graphene/poly-BrNpA FET devices were fabricated through a two-step shadow mask process[38] and the subsequent phosphor coating as follows. First, graphene was etched into an array of channels by magnetic-assisted UV ozonation under irradiation of a xenon excimer lamp (λ = 172 nm). Then, Cr/Au electrodes (5/90 nm) were deposited using a vacuum thermal evaporator. Finally, a 2 wt % poly-BrNpA aqueous solution was dropped on graphene channels and dried by natural evaporation to obtain hybrid graphene/poly-BrNpA FET devices. Herein, the poly-BrNpA powder was synthesized by a radical binary copolymerization of acrylamide and 4-bromo-1, 8-naphthalic anhydride derivative.[28] A KLA-Tencor P7 surface profiler was used to measure the thickness of each layer.

UV Rewritable Photodiode Fabrication and Electronic/Optoelectronic Measurements. A specially equipped fluorescence microscope (Olympus BX61), as schematically illustrated in the configuration (Figure S1), was used to modify charge carrier doping, obtain PL images, and measure the electronic/optoelectronic properties of graphene-based devices. A high-pressure mercury lamp

DOI: 10.1021/acsami.9b14461
ACS Appl. Mater. Interfaces 2019, 11, 43351−43358

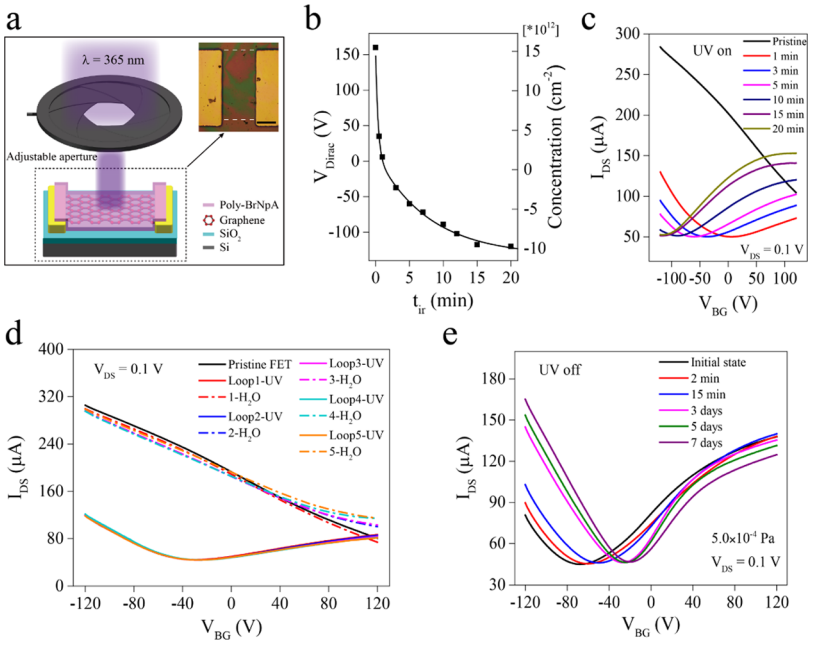

Figure 2. Electrical transport changes in the hybrid graphene/poly-BrNpA FET device upon UV irradiation (λ = 365 nm) and the subsequent H_2O adsorption. (a) Schematic illustration of modifying charge carrier doping in graphene/poly-BrNpA FET device under moderate UV irradiation. Its optical topography is shown in the inset with the scale bar of 100 μm. (b) Dirac point and charge carrier concentration vs t_{ir} for the FET device. The Dirac point at t_{ir} = 0 is an estimated value. (c) Electrical transport curves as a function of t_{ir} when V_{DS} = 0.1 V. (d) Repeatability of the electrical transport varying with five loops of UV irradiation and H_2O adsorption. (e) Electrical transport stability of the UV-irradiated FET device in a high-vacuum environment.

(with three emission lines at 365, 448, and 546 nm) and three semiconductor lasers (473, 532, and 671 nm) were used as light sources. In specific, the 365 nm mercury line, with its spot size tuned through an adjustable aperture, was used to make p−n junctions by local irradiation on the channel. Moreover, the UV beam attenuated to a low intensity was also used for PL imaging along with other two lines at 448 and 546 nm. The laser beams were modulated with a mechanical chopper at 20 Hz. All three lasers were focused individually on the photodiode for photocurrent (I_{ph}) detection, each with a spot size of ∼8.0 μm. The electronic/optoelectronic properties of graphene-based FET devices and p−n junction photodiodes were measured in a flowing nitrogen or other specified atmosphere in combination with Keithley 6430 and 2400 instruments. Water molecules were brought to the poly-BrNpA surface via a flowing humid nitrogen (71% humidity). Light intensity was measured with an optical power meter (Thorlabs PM 100D).

Optical Characterization. The absorption spectra were measured by R1 angle-resolved spectroscopy system equipped with halogen and deuterium light sources (Shanghai Ideaoptics Technology Co., Ltd., China). A confocal micro-Raman/fluorescence spectroscopy (Horiba Jobin Yvon LamRAM HR 800) was used to measure the PL spectrum under the excitation of 325 nm (15× objective, ∼6.0 μm spot size) and 532 nm (50× objective, ∼1.0 μm spot size) lasers. A Varian Cary eclipse spectrophotometer was used to measure the fluorescence/phosphorescence spectrum, and the phosphorescence was discerned from fluorescence emission using a gate time of 0.1 ms in photon collection. A PL spectrometer (Edinburgh instruments FLS1000) was used to measure the PL spectrum and the decay lifetime at a certain wavelength.

RESULTS AND DISCUSSION

The poly-BrNpA polymer is a type of noncrystalline room-temperature phosphor, and its chemical structure is illustrated in Figure 1a. Herein, the heavy bromine (Br) atom can promote a spin−orbit coupling and therefore singlet-to-triplet ($S_1 \rightarrow T_1$) intersystem crossing to attain long lifetime electrons in the excited triplet state for phosphorescence emission.[24] The hydrogen (H) bonding in polymer chains can enhance the phosphorescence intensity, and its breaking when dissolved in water solvent leads to phosphorescence quenching.[24,28]

When treated with moderate UV irradiation (λ = 365 nm, I = 1.386 μW μm^{-2}), the poly-BrNpA film (360 nm thick) changes in its optical properties. Figure 1b plots the evolution of its optical absorption spectrum upon increasing UV irradiation time t_{ir}, wherein a high-quality silica substrate is used. As shown, the poly-BrNpA film has an absorption peak at 347 nm, coincident with that of noncrystalline powder.[28] When combined with graphene, its optical absorption increases in the whole wavelength range (230−800 nm). Then, it weakens at the peak position, while that exceeding 394 nm goes up after 1 min UV irradiation. Upon increasing t_{ir}, the absorption spectrum has a same variation trend but strengthened.

Along with the modified optical absorption, the UV-irradiated poly-BrNpA film changes in its PL emission when excited by UV−vis light as shown in Figure 1c. Blue color appears in the UV-irradiated octagonal regions under weak UV excitation (λ = 365 nm, I = 0.018 μW μm^{-2}), sharply standing out from the surrounding coral background in pristine poly-BrNpA film. Increasing the excitation wavelength to 448 nm (I = 0.036 μW μm^{-2}) and then to 546 nm (I = 0.092 μW μm^{-2}), green and red colors show up sequentially in the same octagonal regions, each forming a sharp color contrast with the dark background. Notably, the PL images get brightened upon the increasing t_{ir} from 1 to 10 min under excitation at any of the three excitation wavelengths.

When excited by a weak 325 nm laser (I = 0.071 μW μm^{-2}), the PL spectral evolution of UV-irradiated poly-BrNpA film is shown in Figure 1d. For the initial pure poly-BrNpA film, there exist two major peaks, i.e., the fluorescence centered at a wavelength of 475 nm and phosphorescence at 580 nm (with a

DOI: 10.1021/acsami.9b14461
ACS Appl. Mater. Interfaces 2019, 11, 43351−43358

shoulder peak at 619 nm). This result is consistent with the poly-BrNpA powder.[28] When the phosphor is coated on a graphene film, the two peaks decrease due to PL quenching. More specific influence of graphene on the PL characteristics of poly-BrNpA film are elaborated in the Supporting Information (Figure S2). For the hybrid structure, the phosphorescence emission at ∼580 nm is inhibited and fluorescence at ∼475 nm enhanced under moderate UV irradiation. Meanwhile, a few fluorescence peaks, absent in the initial poly-BrNpA film, show up and get enhanced upon increasing t_{ir}. We note that a 325 nm laser (I = 0.71 μW μm^{-2}), whose wavelength falls within the absorption band of poly-BrNpA film, can play a same role in modifying its optical properties (Figure S3).

When excited then by a 532 nm laser (I = 0.318 μW μm^{-2}), its PL spectral evolution is shown in Figure 1e. For pure poly-BrNpA film, three weak peaks show up at 552, 596, and 639 nm. The pristine poly-BrNpA film has an optical absorption edge at 400 nm (Figure 1b). When coated on graphene, its PL intensity decreases to one third of its initial value, and each of the three peaks has a red shift of ∼7 nm. The following moderate UV irradiation can prominently improve its PL emission in the whole spectral scope. Specifically, it gets enhanced from eighteen to thirty-eight times at ∼552 nm when t_{ir} increases from 1 to 10 min. The influence of different excitation wavelengths on PL spectrum and how to distinguish between fluorescence and phosphorescence emission are elaborated in the Supporting Information (Figure S4).

Figure 2 shows the electrical transport evolution of a hybrid graphene/poly-BrNpA (55 nm thick) FET device under moderate UV irradiation (λ = 365 nm, I = 1.386 μW μm^{-2}) and its stability in different environmental conditions. The incident UV spot size can be tuned using an adjustable aperture (Figure 2a). When the channel (180 × 380 μm^2) is entirely exposed to UV light, the Dirac point (V_{Dirac}) of graphene shifts from the initial positive toward negative ones upon the increasing t_{ir}, and then saturates at −120 V (Figure 2b). The V_{Dirac} varying as a function of t_{ir} fits an exponential relationship $V_{Dirac} = V_1 \times [e^{-\Upsilon_1 t_{ir}} + e^{-\Upsilon_2 t_{ir}}] + V_0$, where V_1 = 151 V, V_0 = −130 V, Υ_1 = 3.717 min^{-1}, and Υ_2 = 0.145 min^{-1}.

Figure 2c selectively plots the relationship between the drain-source current (I_{DS}) and back-gate voltage (V_{BG}) of the bipolar graphene/poly-BrNpA FET device that underwent different UV irradiation times at a fixed drain-source bias (V_{DS}) of 0.1 V. The charge density n, calculated from the formula $n = C_g V_{Dirac}/e$, changes from +1.15 × 10^{13} cm^{-2} (holes) to −4.32 × 10^{12} cm^{-2} (electrons) upon 5 min UV irradiation, and then saturates at −8.64 × 10^{12} cm^{-2} (electrons) after 20 min UV irradiation with the gate capacitance C_g equal to 115 aF μm^{-2}. The low efficient photoinduced charge transfer at the interface can be attributed to the fact that most of the excited electrons transit to the low ground state via fluorescence and phosphorescence emissions as confirmed in Figure 1d. Further, the photoinduced maximum Fermi energy difference is calculated to be 0.74 eV from the equation $E_F(n) = -\mathrm{sgn}(n)\hbar v_F\sqrt{\pi|n|}$, where $\hbar$ is the reduced Planck constant, and v_F is the Fermi velocity equal to 1.0 × 10^6 m s^{-1}.[39]

The UV-irradiated graphene/poly-BrNpA FET device can restore to its initial p-type doping status within a few seconds under a flush of humid nitrogen (71% humidity) and then reconvert into n-type doping under moderate UV irradiation in nitrogen atmosphere (Figure 2d). The H bonding of poly-BrNpA polymer breaks up via water molecule adsorption and facilitates electron transfer from graphene to the phosphor.[28] The UV-irradiation- and water-adsorption-induced opposite charge doping is reversible and repeatable, accompanied by a slight fluctuation in the conductivity adjacent to the Dirac point mainly stemming from some UV-activated photochemical oxidation of the phosphor and some experimental errors.

The stability of photoinduced charge doping in the hybrid graphene/poly-BrNpA FET device is studied by measuring its electrical transport evolution in a high-vacuum condition (5 × 10^{-4} Pa) as shown in Figure 2e. The Dirac point of graphene first shifts positively and then stabilizes at −21 V at least over seven days. We think the initially unstable Dirac point originates from trace amount of sensitive molecule adsorption like vapor unavoidably resided in the vacuum chamber.[38,40] This viewpoint is supported by its accelerated charge restoration process in ambient atmosphere (Figure S5). Besides, significant increase of current from the beginning to the end of 7 days along with a trend of increasing charge carrier mobilities can be observed. As confirmed in Figures 2d and S5, water adsorption can slightly decrease the charge carrier mobilities. A possible strain release in sample storage can marginally improve its conductivity but with decreased charge carrier mobilities.[41] By excluding influence from water and strain, we think this conductivity change may stem from charge doping of some unknown contamination in the chamber.

The intriguing optical characteristics and charge transfer in the hybrid graphene/poly-BrNpA film can be clarified by the virtue of the electronic band structure as illustrated in Figure 3.

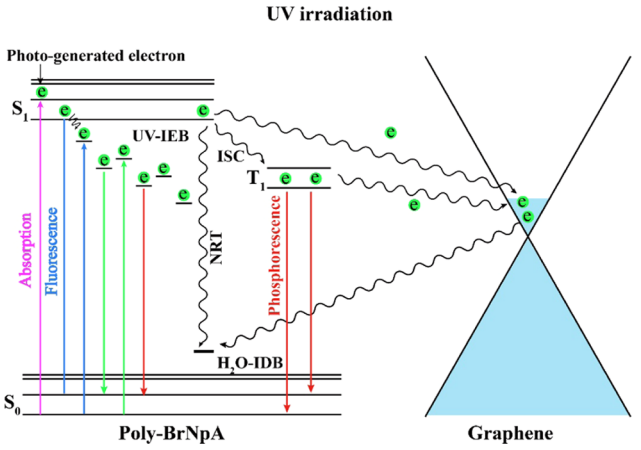

Figure 3. Schematic illustration of electron transfer promoted by UV irradiation and H_2O adsorption in hybrid graphene/poly-BrNpA film by virtue of electronic band structure. UV-IEB, UV irradiation-induced electronic band; H_2O-IDB, H_2O vapor induced defect band; NRT, nonradiative transition, and ISC, intersystem crossing.

We speculate that some quasi-continuous excited states are introduced in the electronic band gap adjacent to the lowest unoccupied molecular orbital (S_1) under the irradiation of moderate UV light (λ < 400 nm). These new electronic states can accommodate electrons excited from ground state or those released from higher excited states.[42] As a consequence, they can modify the optical absorption and emission characteristics of poly-BrNpA film, as well as facilitate electron transfer to the

DOI: 10.1021/acsami.9b14461
ACS Appl. Mater. Interfaces 2019, 11, 43351−43358

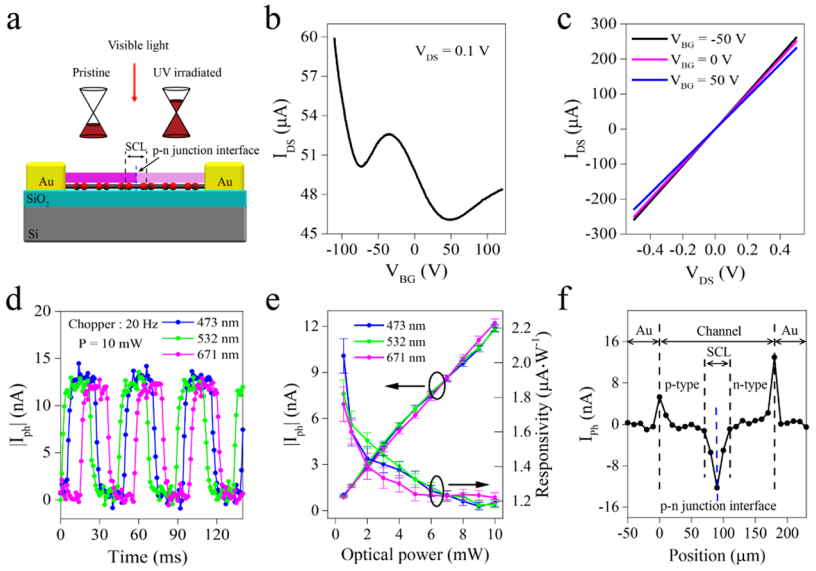

Figure 4. A UV (λ = 365 nm) written graphene/poly-BrNpA lateral p−n junction photodiode and its response to visible light. (a) Schematic of the photodiode formed under UV irradiation for visible light detection. (b) Electrical transport curve of the photodiode. (c) Relationship between drain-source current and bias under different back-gate voltages. (d) Temporal photocurrent dynamics of the photodiode to light pulses at 473, 532, and 671 nm with V_{DS} = V_{BG} = 0 V. (e) Photocurrent and responsivity vs the incident optical power. (f) Photocurrent mapping along the channel axis under 671 nm laser.

underneath graphene. We attribute the exotic optical and electronic changes in the poly-BrNpA film to some kind of UV irradiation-induced irreversible photoisomerization (see the Supporting Information, Figure S6).[22,25]

Humid nitrogen flushing can not only lead to electron transfer from graphene back to UV-irradiated poly-BrNpA but also quench PL intensity in a way different from that in pristine poly-BrNpA film (Figure S7). In this process, the water-adsorption-induced breakup of H bonding can introduce defect states in the band gap close to the highest occupied molecular orbital (S_0) as illustrated in Figure 3. As a result, it facilitates reversible electron transfer from graphene back to the modified poly-BrNpA film.[42]

The peculiar electronic reversibility makes it feasible to realize rewritable p−n junction photodiode in the hybrid graphene/poly-BrNpA FET structure. As schematically illustrated in Figure 4a, a lateral p−n junction photodiode can be made by selectively irradiating UV light (λ = 365 nm, I = 1.386 μW μm^{-2}, t_{ir} = 7 min) on half of the channel from either end. A space charge layer (SCL), composed of positively and negatively charged graphene, forms due to the electron−hole recombination adjacent to the p−n junction interface. The photodiode has two typical Dirac points distributed at −73 and 50 V, as shown in its electrical transport curve (Figure 4b). Hereinto, the less positive Dirac point at 50 V is attained purposefully by the preirradiation of moderate UV light (t_{ir} = 30 s) on the whole channel. The linear current−voltage curves under different gate biases (Figure 4c) indicate that graphene has an ohmic contact with the metal electrodes.

When working in a short-circuit mode under zero gate bias, the lateral graphene/poly-BrNpA photodiode is responsive to visible light at the p−n interface, as shown in the curves of Figure 4d. In specific, it has a photocurrent of 13 nA with the response time of ∼6 ms for all three lasers at 473, 532, and 671 nm each with a fixed incident power of 10 mW. The photocurrent increases monotonically as a function of the optical power, and the corresponding photoresponsivity decreases with the uncertainty of measurement below 6% (Figure 4e). The relationship between the photocurrent and optical power satisfies a power law of $I_{ph} = C_0 P^{\gamma}$, where C_0 is a constant and P is the optical power. For the laser wavelength of 473, 532, and 671 nm, γ takes the values of 0.83, 0.85, and 0.87, respectively. The photoresponsivity appears to be independent of wavelength with a maximum value of 1.94 μA·W^{-1}. The SCL, effective for photodetection, has a length of ∼40 μm as inferred from the photocurrent mapping to 671 nm laser along the channel axis (Figure 4f). For the graphene/poly-BrNpA photodiode, its SCL relies on the electron concentration in photoinduced n-type graphene. The non-uniformity of UV spot, whose energy is mostly distributed in the central area for a Gaussian beam, can incur an increasing length of SCL.

It should be pointed out that the hybrid graphene/poly-BrNpA photodiode appears unstable and eventually converts into a regular FET device with a time elapse in ambient condition (Figure S8a). Accompanying this change, the photoresponse of the photodiode decreases and finally disappears (Figure S8b). More details are described in the Supporting Information.

When a drain-source bias is applied, either positive or negative, the hybrid graphene/poly-BrNpA photodiode has a deteriorated response arising from an increasing noise, even though the photocurrent may appear monotonically enhanced (Figure S9). The photocurrent begins to reverse when an external drain-source bias of +0.2 V is applied, testifying the existence of a built-in electric field in the p−n junction photodiode.[2,11,20]

At zero drain-source bias, the photocurrent of graphene/poly-BrNpA photodiode relies on the back-gate bias in a way conforming with the photovoltaic origination (Figure S9). More specifically, the photoexcited electron−hole pairs are generated in the SCL, and then drift individually toward opposite directions in the built-in electric field.

DOI: 10.1021/acsami.9b14461
ACS Appl. Mater. Interfaces 2019, 11, 43351−43358

The hybrid graphene/poly-BrNpA photodiode can be erased via water adsorption and exhibits rewritable characteristics under moderate UV irradiation as shown in Figure 5. Upon the repetitive loops of UV irradiation and water adsorption, the photodiode appears reproducible with its conductivity marginally fluctuated (Figure 5a). As for its response to visible light, wherein the 532 nm laser is taken for illustration, the rewritable photodiode exhibits repeatable photocurrent and responsivity as a function of the optical power (Figure 5b). The hybrid graphene/poly-BrNpA FET device slightly degrades under repeatable UV irradiation in the course of functioning as a rewritable photodiode, though it does not show any observable degradation when stored in ambient condition for half a year. The unstable nature stems from some photoinduced chemical oxidation of the phosphor because oxygen residues exist unavoidably in the nonpumped nitrogen flowing chamber.

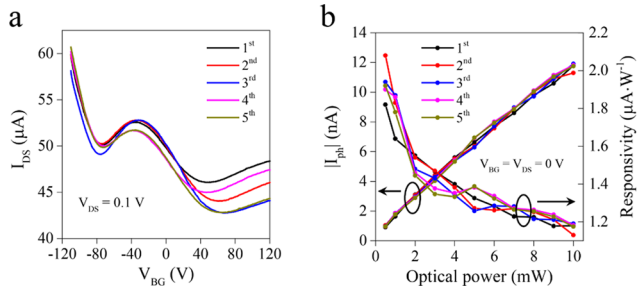

Figure 5. Repeatability of rewritable graphene/poly-BrNpA photodiode. (a) Its electrical transport evolution upon five loops of UV irradiation and H_2O adsorption, and (b) the corresponding photocurrent and responsivity to 532 nm laser as a function of the optical power.

Under UV irradiation, a pure layer of graphene supported on SiO_2/Si substrates turns into n-doped via photoinduced charge transfer as previously reported.[15,18] The poly-BrNpA phosphor, coated on graphene, can highly accelerate the photoinduced charge-transfer process (Figure S10) and provides an efficient way to revert charge carrier doping by water adsorption. When no UV irradiation exerts, the poly-BrNpA coating has an ohmic contact with graphene, since no obvious changes of the Dirac point and charge carrier mobilities can be observed (Figure S11a). Extra Raman spectral analyses show that the G and 2D phonon modes have an average red shift of about 2.5 and 5.6 cm^{-1}, respectively, for graphene covered with the poly-BrNpA (Figure S11b), confirming that it is the strain instead of charge doping that exists at their interface in the dark condition.[41]

The reproducibility of UV rewritable graphene/poly-BrNpA photodiode has been verified with more than ten samples. The thickness of poly-BrNpA phosphor is kept to be ~55 nm with the reason as follows. For a thick poly-BrNpA layer, besides the risk that graphene is unable to convert into n-type doping due to insufficient modification of the phosphor, the increasing strain and decreasing charge carrier mobilities can degrade the hybrid device. For a poly-BrNpA film thinner than 55 nm, it is challenging to make it uniform. More details can be found in the Supporting Information (Figure S12).

For the lateral graphene/poly-BrNpA photodiode, its low responsivity can be traced back to the low optical absorption of graphene at visible wavelengths (2.3%).[29] Meanwhile, the utilization of large-area CVD grown graphene film with low electron/hole mobilities (<700 cm^2 V^{-1} s^{-1}, see Table S1 in the Supporting Information) is also responsible for it by the way of increasing the scattering of electrons and holes and their recombination in the transport process. Further, the high-pressure mercury lamp installed in the optical microscope is unable to write highly spatially resolved p−n junctions. The rewritable photodiode can be improved by two routes: one is to make p−n junctions on high-quality small-area graphene using a UV laser, especially one with a nanoscale resolution equipped on a scanning near-field optical microscope, and the other is to seek more efficient combinations of high-quality two-dimensional materials and photoisomerization polymers.[5−8,16,17] To implement the idea of rewritable p−n junction photodiode in real life, isolation of oxygen molecules can provide a solution to improving the stability of the organic polymers. A technical scheme is proposed with details described in the Supporting Information and illustrated in Figure S13.

CONCLUSIONS

In summary, we have realized UV rewritable lateral p−n junction photodiodes in the hybrid graphene/poly-BrNpA structure. Under moderate UV irradiation, photoisomerization occurred in the poly-BrNpA film can modify its electronic band structure by introducing quasicontinuous electronic states in the band gap. This effect facilitates n-type doping in the graphene/poly-BrNpA film through photoinduced charge transfer and realization of lateral p−n junction photodiode through selective UV irradiation. The hybrid graphene/poly-BrNpA photodiode, stable in vacuum environment, has a responsivity of 1.94 μA·W^{-1} and response time of 6 ms to visible light. The photodiode can be quickly erased by a humid nitrogen flush and exhibits UV rewritable characteristics. This work provides a feasible solution to make rewritable photodetectors by combining graphene with photoisomerization phosphor and an intriguing perspective for developing novel two-dimensional material-based optoelectronic devices.

ASSOCIATED CONTENT

Supporting Information

The Supporting Information is available free of charge on the ACS Publications website at DOI: 10.1021/acsami.9b14461.

Schematic setup for making photodiodes and electronic/optoelectronic measurements; photoluminescence characterization of the poly-BrNpA film; stability of the UV-irradiated graphene/poly-BrNpA FET in ambient condition; identification of photoisomerization in the poly-BrNpA film; influence of water adsorption on PL images of UV-irradiated poly-BrNpA film; stability of the hybrid graphene/poly-BrNpA photodiode in ambient condition; origin of photoresponse in the lateral graphene/poly-BrNpA photodiode; UV irradiation-induced charge doping in pure graphene; influence of the poly-BrNpA coating on graphene properties; influence of the poly-BrNpA thickness on electrical transport property; and schematic of an encapsulated rewritable graphene/poly-BrNpA photodiode (PDF)

AUTHOR INFORMATION

Corresponding Authors

*E-mail: tao.haihua@sjtu.edu.cn (H.T.).
*E-mail: xfchen@sjtu.edu.cn (X.C.).

ORCID

Haihua Tao: 0000-0002-1111-8181

DOI: 10.1021/acsami.9b14461
ACS Appl. Mater. Interfaces 2019, 11, 43351−43358

Xiang Ma: 0000-0002-8679-4491
Zhenhua Ni: 0000-0002-6316-2256
He Tian: 0000-0003-3547-7485

Notes

The authors declare no competing financial interest.

■ ACKNOWLEDGMENTS

This work was supported by National Natural Science Foundation of China (Grant Nos. 11204173, 11874261, 21788102, and 21722603) and Shanghai Municipal Natural Science Foundation (Grant No. 18ZR1419100). We thank Prof. D. Qian, Prof. Y. Dan from Shanghai Jiao Tong University (SJTU) and Prof. H. Peng and Prof. K. Liu from Peking University for constructive discussion. We thank Prof. X. Xie from Shanghai Institute of Microsystem and Information Technology (CAS), Prof. Y. Zhang, Prof. L. Shi from Fudan University, and Prof. Z. Sheng, Prof. Z. Shi from SJTU for their support. We thank L. He, R. Wang from Instrumental Analysis Center (SJTU) and Y. Wang from Advanced Electronic Materials and Devices (SJTU) for their technical support.

■ REFERENCES

(1) Mueller, T.; Xia, F.; Avouris, P. Graphene Photodetectors for High-Speed Optical Communications. *Nat. Photonics* **2010**, *4*, 297−301.
(2) Yan, K.; Wu, D.; Peng, H.; Jin, L.; Fu, Q.; Bao, X.; Liu, Z. Modulation-Doped Growth of Mosaic Graphene with Single-Crystalline p-n Junctions for Efficient Photocurrent Generation. *Nat. Commun.* **2012**, *3*, No. 1280.
(3) Wang, G.; Zhang, M.; Chen, D.; Guo, Q.; Feng, X.; Niu, T.; Liu, X.; Li, A.; Lai, J.; Sun, D.; Liao, Z.; Wang, Y.; Chu, P. K.; Ding, G.; Xie, X.; Di, Z.; Wang, X. Seamless Lateral Graphene p-n Junctions Formed by Selective in situ Doping for High-Performance Photodetectors. *Nat. Commun.* **2018**, *9*, No. 5168.
(4) Gabor, N. M.; Song, J. C.; Ma, Q.; Nair, N. L.; Taychatanapat, T.; Watanabe, K.; Taniguchi, T.; Levitov, L. S.; Jarillo-Herrero, P. Hot Carrier-Assisted Intrinsic Photoresponse in Graphene. *Science* **2011**, *334*, 648−652.
(5) Wang, W. H.; Nan, H. Y.; Liu, Q.; Liang, Z.; Yu, Z. H.; Liu, F. Y.; Hu, W. D.; Zhang, W.; Wang, X. R.; Ni, Z. H. Distinct Photoresponse in Graphene Induced by Laser Irradiation. *Appl. Phys. Lett.* **2015**, *106*, No. 021121.
(6) Seo, B. H.; Youn, J.; Shim, M. Direct Laser Writing of Air-Stable p-n Junctions in Graphene. *ACS Nano* **2014**, *8*, 8831−8836.
(7) Ho, P. H.; Li, S. S.; Liou, Y. T.; Wen, C. Y.; Chung, Y. H.; Chen, C. W. Wavelength-Selective Dual p-and n-Type Carrier Transport of an Organic/Graphene/Inorganic Heterostructure. *Adv. Mater.* **2015**, *27*, 282−287.
(8) De Sanctis, A.; Jones, G. F.; Wehenkel, D. J.; Bezares, F.; Koppens, F. H. L.; Craciun, M. F.; Russo, S. Extraordinary Linear Dynamic Range in Laser-Defined Functionalized Graphene Photodetectors. *Sci. Adv.* **2017**, *3*, No. e1602617.
(9) Konstantatos, G.; Badioli, M.; Gaudreau, L.; Osmond, J.; Bernechea, M.; Garcia de Arquer, F. P.; Gatti, F.; Koppens, F. H. L. Hybrid Graphene-Quantum Dot Phototransistors with Ultrahigh Gain. *Nat. Nanotechnol.* **2012**, *7*, 363−368.
(10) Qin, S.; Chen, X.; Du, Q.; Nie, Z.; Wang, X.; Lu, H.; Wang, X.; Liu, K.; Xu, Y.; Shi, Y.; Zhang, R.; Wang, F. Sensitive and Robust Ultraviolet Photodetector Array Based on Self-Assembled Graphene/C_{60} Hybrid Films. *ACS Appl. Mater. Interfaces* **2018**, *10*, 38326−38333.
(11) Williams, J. R.; DiCarlo, L.; Marcus, C. M. Quantum Hall Effect in a Gate Controlled p-n Junction of Graphene. *Science* **2007**, *317*, 638−641.
(12) Alon, H.; Stern, C.; Kirshner, M.; Sinai, O.; Wasserman, M.; Selhorst, R.; Gasper, R.; Ramasubramaniam, A.; Emrick, T.; Naveh, D. Lithographically Patterned Functional Polymer-Graphene Hybrids for Nanoscale Electronics. *ACS Nano* **2018**, *12*, 1928−1933.
(13) Zhou, Y.; Jadwiszczak, J.; Keane, D.; Chen, Y.; Yu, D.; Zhang, H. Programmable Graphene Doping via Electron Beam Irradiation. *Nanoscale* **2017**, *9*, 8657−8664.
(14) Mulyana, Y.; Uenuma, M.; Okamoto, N.; Ishikawa, Y.; Yamashita, I.; Uraoka, Y. Creating Reversible p-n Junction on Graphene through Ferritin Adsorption. *ACS Appl. Mater. Interfaces* **2016**, *8*, 8192−8200.
(15) Tiberj, A.; Rubio-Roy, M.; Paillet, M.; Huntzinger, J. R.; Landois, P.; Mikolasek, M.; Contreras, S.; Sauvajol, J. L.; Dujardin, E.; Zahab, A. A. Reversible Optical Doping of Graphene. *Sci. Rep.* **2013**, *3*, No. 2355.
(16) Ju, L.; Velasco, J., Jr; Huang, E.; Kahn, S.; Nosiglia, C.; Tsai, H. Z.; Yang, W.; Taniguchi, T.; Watanabe, K.; Zhang, Y.; Zhang, G.; Crommie, M.; Zettl, A.; Wang, F. Photoinduced Doping in Heterostructures of Graphene and Boron Nitride. *Nat. Nanotechnol.* **2014**, *9*, 348−352.
(17) Neumann, C.; Rizzi, L.; Reichardt, S.; Terrés, B.; Khodkov, T.; Watanabe, K.; Taniguchi, T.; Beschoten, B.; Stampfer, C. Spatial Control of Laser-Induced Doping Profiles in Graphene on Hexagonal Boron Nitride. *ACS Appl. Mater. Interfaces* **2016**, *8*, 9377−9383.
(18) Luo, Z.; Pinto, N. J.; Davila, Y.; Charlie Johnson, A. T. Controlled Doping of Graphene Using Ultraviolet Irradiation. *Appl. Phys. Lett.* **2012**, *100*, No. 253108.
(19) Kim, Y. D.; Bae, M. H.; Seo, J. T.; Kim, Y. S.; Kim, H.; Lee, J. H.; Ahn, J. R.; Lee, S. W.; Chun, S. H.; Park, Y. D. Focused-Laser-Enabled p-n Junctions in Graphene Field-Effect Transistors. *ACS Nano* **2013**, *7*, 5850−5857.
(20) Iqbal, M. Z.; Siddique, S.; Iqbal, M. W.; Eom, J. Formation of p-n Junction with Stable p-doping in Graphene Field Effect Transistors Using Deep UV Irradiation. *J. Mater. Chem. C* **2013**, *1*, 3078−3083.
(21) Irvin, P.; Ma, Y.; Bogorin, D. F.; Cen, C.; Bark, C. W.; Folkman, C. M.; Eom, C. B.; Levy, J. Rewritable Nanoscale Oxide Photodetector. *Nat. Photonics* **2010**, *4*, 849−852.
(22) Irie, M.; Kobatake, S.; Horichi, M. Reversible Surface Morphology Changes of a Photochromic Diarylethene Single Crystal by Photoirradiation. *Science* **2001**, *291*, 1769−1772.
(23) Hou, L.; Zhang, X.; Cotella, G. F.; Carnicella, G.; Herder, M.; Schmidt, B. M.; Patzel, M.; Hecht, S.; Cacialli, F.; Samorì, P. Optically Switchable Organic Light-Emitting Transistors. *Nat. Nanotechnol.* **2019**, *14*, 347−353.
(24) Raymo, F. M.; Tomasulo, M. Electron and Energy Transfer Modulation with Photochromic Switches. *Chem. Soc. Rev.* **2005**, *34*, 327−336.
(25) Gu, F.; Zhang, C.; Ma, X. Photo-Modulating Multicolor Photoluminescence Including White-Light Emission from a Photochromic Copolymer. *Macromol. Rapid Commun.* **2019**, *40*, No. 1800751.
(26) Bolton, O.; Lee, K.; Kim, H. J.; Lin, K. Y.; Kim, J. Activating Efficient Phosphorescence from Purely Organic Materials by Crystal Design. *Nat. Chem.* **2011**, *3*, 205−210.
(27) Gu, L.; Shi, H.; Bian, L.; Gu, M.; Ling, K.; Wang, X.; Ma, H.; Cai, S.; Ning, W.; Fu, L.; Wang, H.; Wang, S.; Gao, Y.; Yao, W.; Huo, F.; Tao, Y.; An, Z.; Liu, X.; Huang, W. Colour-Tunable Ultra-Long Organic Phosphorescence of a Single-Component Molecular Crystal. *Nat. Photonics* **2019**, *13*, 406−411.
(28) Chen, H.; Yao, X.; Ma, X.; Tian, H. Amorphous, Efficient, Room-Temperature Phosphorescent Metal-Free Polymers and Their Applications as Encryption Ink. *Adv. Opt. Mater.* **2016**, *4*, 1397−1401.
(29) Koppens, F. H. L.; Mueller, T.; Avouris, P.; Ferrari, A. C.; Vitiello, M. S.; Polini, M. Photodetectors Based on Graphene, Other Two-Dimensional Materials and Hybrid Systems. *Nat. Nanotechnol.* **2014**, *9*, 780−793.
(30) Liu, C.; Xu, X.; Qiu, L.; Wu, M.; Qiao, R.; Wang, L.; Wang, J.; Niu, J.; Liang, J.; Zhou, X.; Zhang, Z.; Peng, M.; Gao, P.; Wang, W.; Bai, X.; Ma, D.; Jiang, Y.; Wu, X.; Yu, D.; Wang, E.; Xiong, J.; Ding,

DOI: 10.1021/acsami.9b14461
ACS Appl. Mater. Interfaces 2019, 11, 43351−43358

F.; Liu, K. Kinetic Modulation of Graphene Growth by Fluorine through Spatially Confined Decomposition of Metal Fluorides. *Nat. Chem.* **2019**, *11*, 730−736.
(31) Yuan, H.; Liu, X.; Afshinmanesh, F.; Li, W.; Xu, G.; Sun, J.; Lian, B.; Curto, A. G.; Ye, G.; Hikita, Y.; Shen, Z.; Zhang, S. C.; Chen, X.; Brongersma, M.; Hwang, H. Y.; Cui, Y. Polarization-Sensitive Broadband Photodetector Using a Black Phosphorus Vertical p−n Junction. *Nat. Nanotechnol.* **2015**, *10*, 707−713.
(32) Lee, J. S.; Choi, S. H.; Yun, S. J.; Kim, Y. I.; Boandoh, S.; Park, J. H.; Shin, B. G.; Ko, H.; Lee, S. H.; Kim, Y. M.; Lee, Y. H.; Kim, K. K.; Kim, S. M. Wafer-Scale Single-Crystal Hexagonal Boron Nitride Film via Self-Collimated Grain Formation. *Science* **2018**, *362*, 817−821.
(33) Wang, L.; Xu, X.; Zhang, L.; Qiao, R.; Wu, M.; Wang, Z.; Zhang, S.; Liang, J.; Zhang, Z.; Zhang, Z.; Chen, W.; Xie, X.; Zong, J.; Shan, Y.; Guo, Y.; Willinger, M.; Wu, H.; Li, Q.; Wang, W.; Gao, P.; Wu, S.; Zhang, Y.; Jiang, Y.; Yu, D.; Wang, E.; Bai, X.; Wang, Z. J.; Ding, F.; Liu, K. Epitaxial Growth of a 100-Square-Centimetre Single-Crystal Hexagonal Boron Nitride Monolayer on Copper. *Nature* **2019**, *570*, 91−95.
(34) Li, X.; Cai, W.; An, J.; Kim, S.; Nah, J.; Yang, D.; Piner, R.; Velamakanni, A.; Jung, I.; Tutuc, E.; Banerjee, S. K.; Colombo, L.; Ruoff, R. S. Large-Area Synthesis of High-Quality and Uniform Graphene Films on Copper Foils. *Science* **2009**, *324*, 1312−1314.
(35) Xu, X.; Zhang, Z.; Qiu, L.; Zhuang, J.; Zhang, L.; Wang, H.; Liao, C.; Song, H.; Qiao, R.; Gao, P.; Hu, Z.; Liao, L.; Liao, Z.; Yu, D.; Wang, E.; Ding, F.; Peng, H.; Liu, K. Ultrafast Growth of Single-Crystal Graphene Assisted by a Continuous Oxygen Supply. *Nat. Nanotechnol.* **2016**, *11*, 930−935.
(36) Liang, X.; Sperling, B. A.; Calizo, I.; Cheng, G.; Hacker, C. A.; Zhang, Q.; Obeng, Y.; Yan, K.; Peng, H.; Li, Q.; Zhu, X.; Yuan, H.; Walker, A. R. H.; Liu, Z.; Peng, L.; Richter, C. A. Toward Clean and Crackless Transfer of Graphene. *ACS Nano* **2011**, *5*, 9144−9153.
(37) Li, X.; Zhu, Y.; Cai, W.; Borysiak, M.; Han, B.; Chen, D.; Piner, R. D.; Colombo, L.; Ruoff, R. S. Transfer of Large-Area Graphene Films for High-Performance Transparent Conductive Electrodes. *Nano Lett.* **2009**, *9*, 4359−4363.
(38) Wu, Y.; Tao, H.; Su, S.; Yue, H.; Li, H.; Zhang, Z.; Ni, Z.; Chen, X. Patterning Graphene Film by Magnetic-Assisted UV Ozonation. *Sci. Rep* **2017**, *7*, No. 46583.
(39) Yan, J.; Zhang, Y.; Kim, P.; Pinczuk, A. Electric Field Effect Tuning of Electron-Phonon Coupling in Graphene. *Phys. Rev. Lett.* **2007**, *98*, No. 166802.
(40) Zhang, Z.; Tao, H.; Li, H.; Ding, G.; Ni, Z.; Chen, X. Making Few-Layer Graphene Photoluminescent by UV Ozonation. *Opt. Mater. Express* **2016**, *6*, 3527−3540.
(41) Huang, M.; Pascal, T. A.; Kim, H.; Goddard, W. A., III; Greer, J. R. Electronic-Mechanical Coupling in Graphene from in situ Nanoindentation Experiments and Multiscale Atomistic Simulations. *Nano Lett.* **2011**, *11*, 1241−1246.
(42) Vincenzo, B.; Paola, C.; Alberto, J. *Photochemistry and Photophysics: Concepts, Research, Applications*; Wiley-VCH Verlag GmbH & Co. KGaA: Weinheim, Germany, 2014.

DOI: 10.1021/acsami.9b14461
ACS Appl. Mater. Interfaces 2019, 11, 43351−43358